NANO LETTERS

Letter

pubs.acs.org/NanoLett

Epitaxial Growth of $Mg_xCa_{1-x}O$ on GaN by Atomic Layer Deposition

Xiabing Lou,[†] Hong Zhou,[‡] Sang Bok Kim,[†] Sami Alghamdi,[‡] Xian Gong,[†] Jun Feng,[†] Xinwei Wang,[†] Peide D. Ye,[‡] and Roy G. Gordon*[,†]

[†]Department of Chemistry and Chemical Biology, Harvard University, Cambridge, Massachusetts 02138, United States

[‡]School of Electrical and Computer Engineering and Birck Nanotechnology Center, Purdue University, West Lafayette, Indiana 47906, United States

Supporting Information

ABSTRACT: We demonstrate for the first time that a single-crystalline epitaxial $Mg_xCa_{1-x}O$ film can be deposited on gallium nitride (GaN) by atomic layer deposition (ALD). By adjusting the ratio between the amounts of Mg and Ca in the film, a lattice matched $Mg_xCa_{1-x}O$/GaN(0001) interface can be achieved with low interfacial defect density. High-resolution X-ray diffraction (XRD) shows that the lattice parameter of this ternary oxide nearly obeys Vegard's law. An atomically sharp interface from cross-sectional transmission electron microscopy (TEM) confirmed the high quality of the epitaxy. High-temperature capacitance−voltage characterization showed that the film with composition $Mg_{0.25}Ca_{0.75}O$ has the lowest interfacial defect density. With this optimal oxide composition, a $Mg_{0.25}Ca_{0.75}O$/AlGaN/GaN metal−oxide−semiconductor high-electron-mobility (MOS-HEMT) device was fabricated. An ultrahigh on/off ratio of 10^{12} and a near ideal SS of 62 mV/dec were achieved with this device.

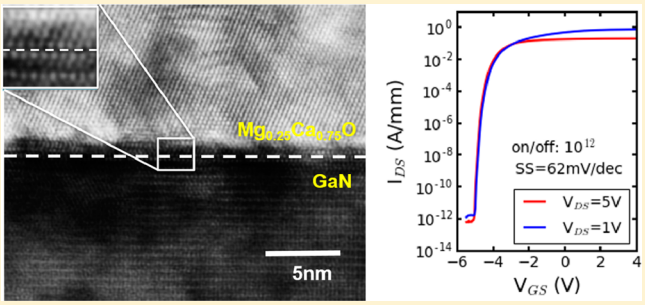

KEYWORDS: *Epitaxy, dielectric, GaN, MOS-HEMT, magnesium calcium oxide*

The wide implementation of solar energy and fast development of electrical vehicles both require more efficient power electronic devices working under high voltage (>600 V), high temperature (>100 °C), and high frequency conditions.[1] Currently, Si-based power devices could not meet these demands due to the small band gap (1.1 eV) and low breakdown field of Si.[2] GaN could replace Si for future power applications because of its higher band gap (3.4 eV) and higher breakdown field. However, unlike Si, the interface trap density between GaN and its native oxide (Ga_2O_3) is huge, which prevents high efficiency modulation of GaN devices. Many alternative dielectrics, such as HfO_2,[3] Al_2O_3,[4] SiO_2,[5] Sc_2O_3,[6] etc., have been employed as dielectrics on GaN in various studies. However, GaN devices with a low defect interface and high quality dielectric have not been achieved with any material.

Recently, our group demonstrated that ALD can grow lanthanum oxide epitaxially on gallium arsenide (GaAs) (111)A surfaces and that the density of interfacial defects is remarkably low.[7] Although the (0001) surface of GaN wurtzite structure has an atomic structure similar to the (111)A surface of GaAs, it is more challenging to apply the same strategy to GaN due to the lack of any lattice matched oxide. We have also reported ALD-Sc_2O_3 growth on AlGaN/GaN-based HEMT devices.[6] Because of the large lattice mismatch between Sc_2O_3 and the substrate (~9%), epitaxial growth could not be achieved. MgO and CaO both have relatively high dielectric constants (MgO 9.8, CaO 11.8) and large band gaps (both 7−8 eV) and thus might be suitable gate oxides for GaN. Moreover, the GaN lattice size lies between those of the MgO and CaO lattices (mismatch −6.5% for MgO and +6.5% for CaO). Therefore, by tuning the composition of $Mg_xCa_{1-x}O$, a lattice match with GaN substrates can be achieved. Hellman et al.[8] demonstrated that epitaxial $Mg_xCa_{1-x}O$ can be grown by molecular beam epitaxy (MBE) on MgO substrates. Later, Paisley et al.[9] and Ren et al.[10] reported that epitaxial $Mg_{0.5}Ca_{0.5}O$ can be grown on GaN with the same method. Measurements on HEMTs with MBE-fabricated MgCaO insulators showed improved gate lag.[11] However, MBE is not applicable to large substrates needed for cost-effective industrial processing. Thus, a more scalable and lower cost method to deposit epitaxial $Mg_xCa_{1-x}O$ is highly desirable.

In this work, we demonstrate that atomic layer deposition (ALD) can form $Mg_xCa_{1-x}O$ epitaxially on GaN(0001). Cross-sectional transmission electron microscopy (TEM) determined the relationship of this heteroepitaxy to be (111) × [011]$Mg_xCa_{1-x}O$//GaN(0001) × [11−20]. High-resolution X-ray diffraction (HRXRD) and electron diffraction (ED) showed that the lattice constants of $Mg_xCa_{1-x}O$ with different compositions are close to the predictions of Vegard's law. Capacitance−voltage (C−V) measurements were employed to study the interfacial defects and $Mg_{0.25}Ca_{0.75}O$ showed the lowest density of defects. Additionally, an ultrahigh on/off ratio

Received: August 29, 2016
Revised: November 16, 2016
Published: November 28, 2016

DOI: 10.1021/acs.nanolett.6b03638
Nano Lett. 2016, 16, 7650−7654

of 10^{12} and a near-ideal subthreshold swing of 62 mV/dec were achieved with $Mg_{0.25}Ca_{0.75}O$ as a gate oxide of GaN MOS-HEMT. This is the first demonstration of epitaxial $Mg_xCa_{1-x}O$ in a GaN/AlGaN/GaN MOS-HEMT device. The results show that the $Mg_xCa_{1-x}O$ dielectric is promising for applications in high-frequency and power electronics.

ALD of $Mg_xCa_{1-x}O$ was carried out in a home-built tubular reactor.[12] Bis(*N*,*N*′-diisopropylacetamidinato)calcium(II) dimer,[13] bis(*N*,*N*′-di-*sec*-butylacetamidinato)magnesium,[14] and H_2O were used as calcium, magnesium, and oxygen sources, respectively. Structural formulas for the Mg and Ca precursors are shown in Figure 1. Three different precursor dosing ratios,

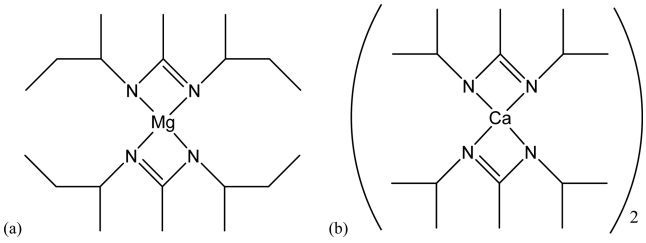

Figure 1. Structures of the metal precursors: (a) bis(*N*,*N*′-di-*sec*-butylacetamidinato)magnesium; (b) bis(*N*,*N*′-diisopropylacetamidinato)calcium(II) dimer.

namely Mg:Ca = 1:1, Mg:Ca = 1:2, and Mg:Ca = 1:3, were employed. The compositions of the resulting films were determined by Rutherford backscattering spectroscopy (RBS) to be $Mg_{0.72}Ca_{0.28}O$, $Mg_{0.51}Ca_{0.49}O$, and $Mg_{0.25}Ca_{0.75}O$, respectively. The detailed growth conditions are summarized in the Supporting Information. The depositions below a substrate temperature of 290 °C were not well crystallized while carbon impurity can be detected at above 330 °C. Therefore, an optimal growth temperature is determined to be 310 °C. The film growth rates with different dosing ratios and the corresponding compositions are summarized in Table 1.

Table 1. Summary of ALD Growth Rates, Compositions, and Lattice Constants of Different $Mg_xCa_{1-x}O$ Films[a]

dosing ratio Mg:Ca	av growth rate (nm/cycle)	composition	lattice constant (nm)	Vagard's law prediction (nm)
CaO	0.075	CaO	0.1389	0.1389
1:3	0.05	$Mg_{0.25}Ca_{0.75}O$	0.134	0.1345
1:2	0.05	$Mg_{0.51}Ca_{0.49}O$	0.133	0.1299
1:1	0.06	$Mg_{0.72}Ca_{0.28}O$	0.128	0.1262
MgO	0.05	MgO	0.1213	0.1213

[a]The composition was measured by Rutherford backscattering (RBS). Lattice constants of $Mg_xCa_{1-x}O$ (222) were measured by HRXRD. MgO and CaO (222) lattice constants were from Crystallography Open Database.

For all three compositions, the growth rates are slightly smaller than a linear combination of the MgO and CaO growth rates, and the Mg contents are higher than their corresponding dosing ratio in the 1:1 and 1:2 cases. This indicates that the MgO cycle might have a hindering effect on the reaction of the CaO deposition cycle. Although MgO and CaO are nearly immiscible at equilibrium below 2000 °C,[15] this solid mixture is kinetically stable up to about 600 °C.[16]

One powerful method to examine the epitaxial film quality is cross-sectional TEM imaging. Figure 2 summarizes the cross-

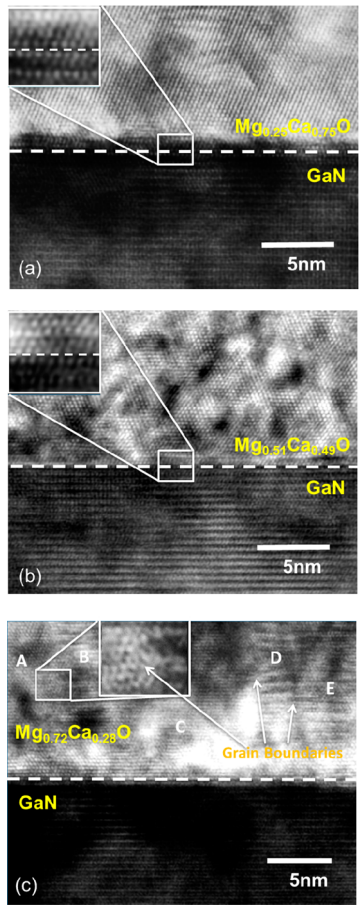

Figure 2. Cross-sectional TEM of $Mg_xCa_{1-x}O$ films grown on GaN(0001) surface. (a) $Mg_{0.25}Ca_{0.75}O$/GaN; (b) $Mg_{0.51}Ca_{0.49}O$/GaN; (c) $Mg_{0.72}Ca_{0.28}O$/GaN; grain boundaries can be found between each region labeled with letters. The enlarged grain boundary between region A and B shows both darkness contrast as well as pattern difference. Region B is showing a three line repeating pattern, which indicates two different orientation grains are overlapping together. A similar pattern can also be found in regions D and E.

section TEM images of three different $Mg_xCa_{1-x}O$/GaN samples. Since GaN and $Mg_xCa_{1-x}O$ have different crystal structures, their lattice patterns in TEM are different. The GaN region shows a distinctive three atomic line periodicity pattern in the vertical direction while $Mg_xCa_{1-x}O$ does not have this feature. All three samples show sharp interfaces without any interfacial layer. The nearly perfect single crystal lattices in Figure 2a,b confirmed the high quality of epitaxy of $Mg_{0.25}Ca_{0.75}O$ and $Mg_{0.51}Ca_{0.49}O$ on GaN. On the other hand, the grain boundaries in Figure 2c indicate that a highly textured $Mg_{0.72}Ca_{0.28}O$ film is formed on GaN. The well-defined film spots in the diffraction pattern (Figure S2) also confirmed the high quality of epitaxial $Mg_{0.25}Ca_{0.75}O$ and $Mg_{0.51}Ca_{0.49}O$ films while the $Mg_{0.72}Ca_{0.28}O$ film has some textured features. Moreover, from the diffraction pattern, the zone axis of the GaN substrate in these TEM images is [11−20], while the film zone axis can be determined as [011]. Therefore, the epitaxial relation between the film and substrate is (111) × [0−11] $Mg_xCa_{1-x}O$ //GaN(0001) × [11−20].

In order to study the lattice mismatch between $Mg_xCa_{1-x}O$ film and GaN substrate, coupled $2\theta-\omega$ HRXRD scans were employed. Both GaN(0004) and $Mg_xCa_{1-x}O$(222) peaks are seen in all three samples (Figure 3a). The absence of MgO and

DOI: 10.1021/acs.nanolett.6b03638
Nano Lett. 2016, 16, 7650−7654

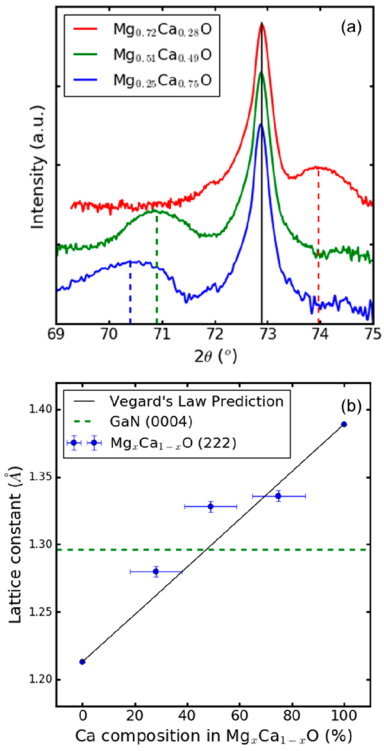

Figure 3. Lattice constant study by HRXRD. (a) HRXRD study of $Mg_xCa_{1-x}O$/GaN film. The black vertical line is the peak position of GaN(0004) diffraction. The dashed lines represent the peak positions of the $Mg_xCa_{1-x}O$ (222) diffractions. (b) Vegard's law predicted lattice constant vs XRD measured polycrystalline $Mg_xCa_{1-x}O$ (222) lattice constants. The green dashed line is the lattice constant that matches the GaN(0004) lattice.

CaO peaks indicates that phase separation into the two binaries has not occurred. The $Mg_xCa_{1-x}O$(222) peak shifts to lower 2θ position as the Ca content increases. Both measured lattice constants and the calculated lattice constants based on Vegard's law are plotted in Figure 3b. Assuming a fully relaxed heteroepitaxial relation at the interface and considering the epitaxial relationship between the film and the substrate, the out-of-plane lattice mismatch can be defined as $(a_{MgCaO(222)} - a_{GaN(0004)})/a_{GaN(0004)}$.[7] The mismatch is −1.2% for $Mg_{0.72}Ca_{0.28}O$, +2.4% for $Mg_{0.51}Ca_{0.49}O$, and +3.1% for $Mg_{0.25}Ca_{0.75}O$. Similar lattice mismatch values obtained from in-plane fast Fourier transformation analysis of TEM cross-sectional images also confirmed the relaxed interface (Figure S8). Despite the larger lattice mismatch, $Mg_{0.51}Ca_{0.49}O$ and $Mg_{0.25}Ca_{0.75}O$ show nearly perfect epitaxy while $Mg_{0.72}Ca_{0.28}O$, with a smaller mismatch, exhibits a textured structure. Such results indicate that there might be factors other than mismatch affecting the epitaxial quality.

Although MgO and CaO are immiscible with each other below 2000 °C,[15] previous reports[9,17] have shown that $Mg_xCa_{1-x}O$ can be grown by MBE at lower temperature without phase separation. In order to examine the microscopic crystallinity and phase composition of the $Mg_xCa_{1-x}O$ films deposited by this ALD method, transmission electron microscopy (TEM) was employed. As shown in the Supporting Information, the ring diffraction pattern in Figure S1b clearly indicates that film is polycrystalline on SiN_x. The relative positions between different diffraction rings in the electron diffraction pattern are in accord with the face-centered cubic (FCC) standard pattern. This indicates that the $Mg_xCa_{1-x}O$ shares the same rock salt structure with MgO and CaO. Additionally, the values of the lattice spacings lie in between the corresponding spacings in MgO and CaO, showing that the $Mg_xCa_{1-x}O$ film is a uniform alloy of the two components without phase separation.

In summary of the above structural characterizations, $Mg_xCa_{1-x}O$ films deposited by ALD were proved to be epitaxial on GaN by both TEM and XRD. Cross-sectional TEM revealed near perfect epitaxy of $Mg_{0.51}Ca_{0.49}O$ and $Mg_{0.25}Ca_{0.75}O$ on GaN. However, although a smaller lattice mismatch was found in $Mg_{0.72}Ca_{0.28}O$/GaN, the epitaxy was not as perfect as for the other two compositions. Therefore, lattice mismatch might not be the only parameter affecting the quality of epitaxy.

$Mg_xCa_{1-x}O$/GaN MOS-capacitor devices were fabricated to examine the electrical performance by capacitance−voltage and conductance−voltage measurements. Since GaN has a wide band gap of 3.4 eV, a room temperature C−V does not effectively probe defects near the middle of the bandgap. Therefore, the MOS-capacitors were measured at 150 °C as well as at room temperature. Because of the hydroscopic nature of $Mg_xCa_{1-x}O$, 5 nm of Al_2O_3 was deposited as a capping layer to keep moisture away from the $Mg_xCa_{1-x}O$ layer. An amorphous Al_2O_3/GaN MOS was also prepared for comparison. A "top-to-top" capacitor structure was used to measure the capacitance due to the insulating sapphire substrate under the GaN (Figure S3). In this measurement, the positive probe is placed in contact with the gate electrode while the negative probe is in contact with the large area of GaN covered by aluminum metal. Since the gate has a serial connection with the large area, the measured capacitance is given by $1/C_m = 1/C_g + 1/C_l$, where C_m is the capacitance measured by the LCR meter, C_g is the capacitance of the gate, and C_l is the capacitance of the larger area. Since $C_l \gg C_g$, the measured capacitance is dominated by the gate: $C_m \approx C_g$.

The measured room temperature and high temperature C−V curves from three $Mg_xCa_{1-x}O$/GaN samples as well as an Al_2O_3/GaN sample are summarized in Figure 4. In room temperature studies (Figure 4a−c), very small (<6%) frequency dispersion can be seen in the depletion region for all three $Mg_xCa_{1-x}O$ samples, while there is a 20% dispersion in the same region in the Al_2O_3/GaN sample (Figure 4d). In the absence of interface traps, dispersion should not occur. Therefore, the reduced dispersion in the three $Mg_xCa_{1-x}O$ samples compared to the Al_2O_3 sample qualitatively indicates that the epitaxial film did reduce the number of interfacial traps. Because of the low interfacial trap density, a numerical value for D_{it} could not be extracted from the room temperature C−V measurements. During the C−V measurement, the Fermi level is moved deeper in the band gap at a higher temperature; thus, defect information can be obtained over a wider range of energies within the band gap.[18] In the C−V data taken at 150 °C (Figure 4e−h), the frequency dispersion remained relatively small (<6%) for all three $Mg_xCa_{1-x}O$ samples while the dispersion in Al_2O_3/GaN is as large as 100%. The smaller frequency dispersion at high temperature indicates that the $Mg_xCa_{1-x}O$ film effectively reduced the interfacial trap density near the midgap region compared to Al_2O_3. In order to measure the D_{it} values quantitatively, the conductance method was employed since the Terman method is considered less sensitive[19] and the Gray−Brown method is not applicable to III−V semiconductors.[20] The detailed measurement procedure

DOI: 10.1021/acs.nanolett.6b03638
Nano Lett. 2016, 16, 7650−7654

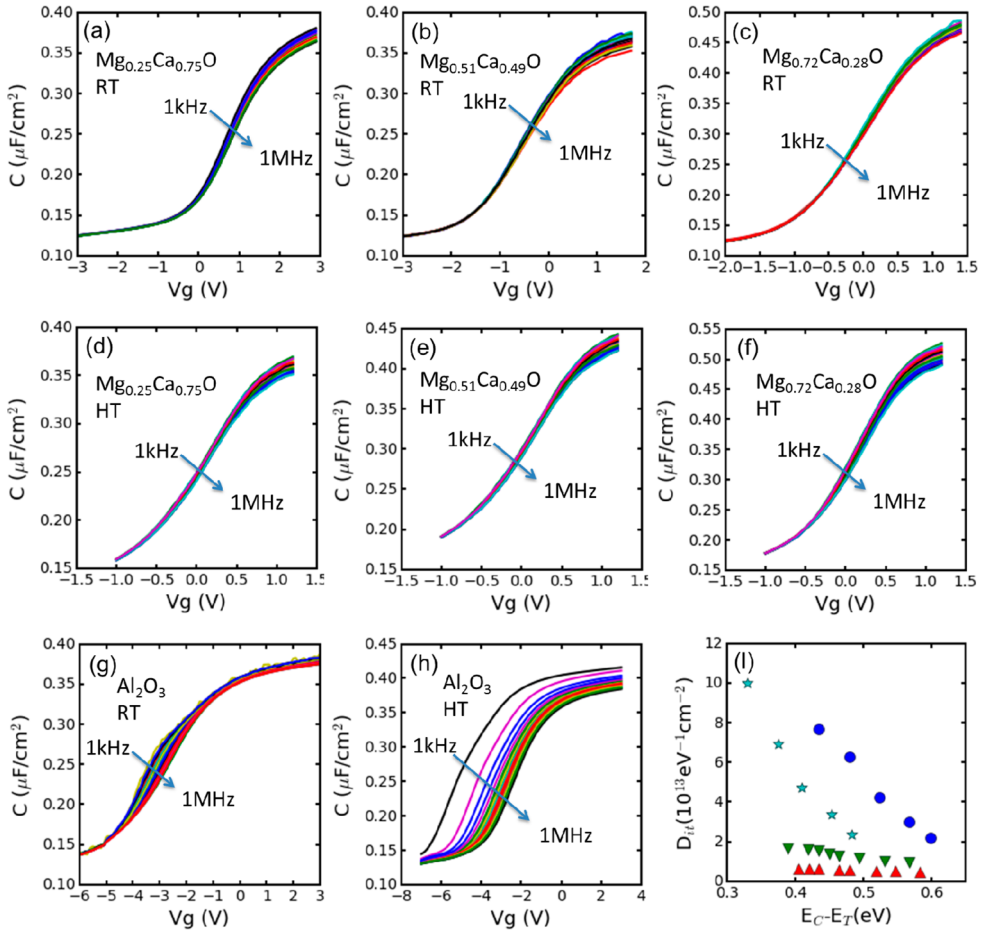

Figure 4. *C*−*V* measurements for $Mg_xCa_{1-x}O$/GaN and Al_2O_3/GaN samples. The frequency ranges of all samples are from 1 kHz to 1 MHz. (a) 20 °C Al_2O_3(5 nm)/$Mg_{0.25}Ca_{0.75}O$(15 nm)/GaN; (b) 20 °C Al_2O_3(5 nm)/$Mg_{0.51}Ca_{0.49}O$(15 nm)/GaN; (c) 20 °C Al_2O_3(5 nm)/$Mg_{0.72}Ca_{0.28}O$(15 nm)/GaN; (d) 150 °C Al_2O_3(5 nm)/$Mg_{0.25}Ca_{0.75}O$(15 nm)/GaN; (e) 150 °C Al_2O_3(5 nm)/$Mg_{0.51}Ca_{0.49}O$(15 nm)/GaN; (f) 150 °C Al_2O_3(5 nm)/$Mg_{0.72}Ca_{0.28}O$(15 nm)/GaN; (g) 20 °C Al_2O_3(20 nm)/GaN for comparison; (h) 150°C Al_2O_3(20nm)/GaN. (i) D_{it} summary of four samples determined by the conductance method: Al_2O_3(20 nm)/GaN (light blue star), Al_2O_3(5 nm)/$Mg_{0.72}Ca_{0.28}O$(15 nm)/GaN (blue circles), Al_2O_3(5 nm)/$Mg_{0.51}Ca_{0.49}O$(15 nm)/GaN (green down triangle), and Al_2O_3(5 nm)/$Mg_{0.25}Ca_{0.75}O$(15 nm)/GaN (red up triangles).

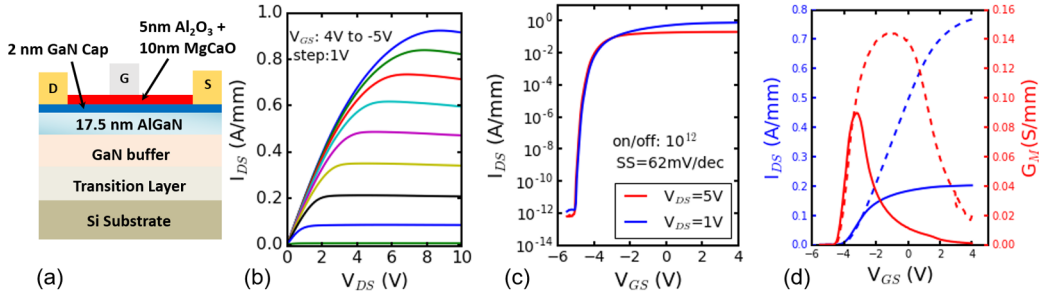

Figure 5. MOS-HEMT device performance characterization. (a) Schematic of the $Mg_xCa_{1-x}O$ MOS-HEMT device. (b) Transfer characteristics of the $Mg_{0.25}Ca_{0.75}O$/GaN/AlGaN/GaN MOS-HEMT device. (c) *I*−*V* characteristics comparison between two different source drain voltage. (d) Conductivity and current vs gate voltage study. Solid lines represent V_{DS} = 5 V; dashed lines represent V_{DS} = 1 V.

and conductance data are summarized in the Supporting Information (Figure S5).[18] The measured values of D_{it} are summarized in Figure 4i. Two of the samples with epitaxial films show the lowest D_{it} values, while the textured sample has about 1 order of magnitude higher interfacial trap density. Although the lattice mismatch of the $Mg_{0.25}Ca_{0.75}O$ sample is slightly larger than that of the other two $Mg_xCa_{1-x}O$ samples, the measured D_{it} level is the lowest (~5 × 10^{12} eV^{-1} cm^{-2}). One possible explanation is that during the early ALD cycles, the Ca growth rate is smaller than that of the Mg. Thus, the Ca content near the interface is lower than in the bulk $Mg_xCa_{1-x}O$ film. Another possible explanation is that a trace amount of $Mg(OH)_2$ may also cause interfacial traps, while adding more Ca content may help reduce the number of hydroxyl groups and therefore reduce the D_{it} level. The dielectric constant of the $Mg_{0.25}Ca_{0.75}O$ film derived from the C−V measurement is 10, which is close to the permittivities of MgO and CaO.

The ultimate goal of developing this material is implementing $Mg_xCa_{1-x}O$ into GaN MOS-HEMT devices with unprecedented oxide/semiconductor interface quality. A

DOI: 10.1021/acs.nanolett.6b03638
Nano Lett. 2016, 16, 7650−7654

schematic cross section of such a device is shown in Figure 5a. The fabrication process is summarized in the Supporting Information. The $Mg_{0.25}Ca_{0.75}O$ film was used as the gate dielectric in this study due to its lower D_{it}. The gate oxide stack is Al_2O_3(5 nm)/$Mg_{0.25}Ca_{0.75}O$(10 nm). Well-behaved I_d-V_{ds} and linear-scale I_d-V_{gs} curves (Figure 5b,d) show the good control capability of the GaN MOS-HEMT. Figure 5c shows the transfer characteristics in a log-scale plot at V_{ds} = 1 and 5 V. This device possesses an ultrahigh on/off ratio 10^{12} due to the high quality interface. Thus, the channel can be shut off completely. This value is 2 orders of magnitude higher than those HEMT devices with Al_2O_3 passivation.[21] In addition to the ultrahigh on/off ratio, the GaN MOS-HEMT also possesses a near ideal subthreshold swing (SS) of 62 mV/dec, further confirming the high quality interface between GaN and the $Mg_{0.25}Ca_{0.75}O$ layer.[22] The successful implementation of the $Mg_{0.25}Ca_{0.75}O$ into a GaN MOS-HEMT shows that it is promising for use in GaN MOS technology.

Epitaxial $Mg_xCa_{1-x}O$ films have been successfully grown on GaN (0001) surfaces using ALD for the first time. The crystallographic relationship of this heteroepitaxy has been studied in detail. Moreover, the potential of applying this unprecedentedly high-quality dielectric film has been evaluated with $C-V$ characterization, revealing that the density of defects is affected by not only the lattice mismatch but also by the composition of the film. $Mg_{0.25}Ca_{0.75}O$ is found to provide the interface with the fewest traps, and the MOS-HEMT made from it exhibits an ultrahigh on/off ratio of 10^{12} and a near ideal SS of 62 mV/dec. Thus, we believe this epitaxial $Mg_xCa_{1-x}O$ film can provide improved high-frequency and high-power electronics in the future.

■ ASSOCIATED CONTENT

Supporting Information

The Supporting Information is available free of charge on the ACS Publications website at DOI: 10.1021/acs.nanolett.6b03638.

Methods, TEM diffraction patterns of $Mg_xCa_{1-x}O$/GaN, MOS-HEMT and MOS-capacitor fabrication, ac conductance method to extract D_{it} (PDF)

■ AUTHOR INFORMATION

Corresponding Author

*(R.G.G.) E-mail: gordon@chemistry.harvard.edu.

ORCID

Xiabing Lou: 0000-0003-4402-3207

Peide D. Ye: 0000-0001-8466-9745

Present Address

X.W.: School of Advanced Materials, Shenzhen Graduate School, Peking University, Shenzhen 518055, China.

Notes

The authors declare no competing financial interest.

■ ACKNOWLEDGMENTS

The work at Harvard University is supported by the Center for the Next Generation of Materials by Design, an Energy Frontier Research Center funded by the U.S. DOE, Office of Science. The work at Purdue University is supported in part by AFOSR (FA9550-12-1-0180) and in part by Award N000141512833 from ONR. Some of the work was performed at Harvard University's Center for Nanoscale Systems (CNS), a member of the National Nanotechnology Infra-Structure Network (NNIN), and at Harvard's X-ray laboratory. We thank Kelson Chabak from AFRL for providing the high-quality AlGaN/GaN on Si wafers for this research.

■ REFERENCES

(1) Hensel, A.; Wilhelm, C.; Kranzer, D. *IEEE Int. Power Electron. Motion Control Conf.* **2012**, DS3d.4-1−DS3d.4-5.

(2) Ikeda, N.; Li, J.; Kato, S.; Masuda, M.; Yoshida, S. *Furukawa Rev.* **2006**, No. No. 29, 1−6.

(3) Tang, Z. J.; Li, R.; Yin, J. *J. Mater. Sci.: Mater. Electron.* **2014**, *25* (1), 152−156.

(4) Kang, H.-S.; Reddy, M. S. P.; Kim, D.-S.; Kim, K.-W.; Ha, J.-B.; Lee, Y. S.; Choi, H.-C.; Lee, J.-H. *J. Phys. D: Appl. Phys.* **2013**, *46* (15), 155101.

(5) Huang, W.; Khan, T.; Chow, T. P. *J. Electron. Mater.* **2006**, *35* (4), 726−732.

(6) Wang, X.; Saadat, O. I.; Xi, B.; Lou, X.; Molnar, R. J.; Palacios, T.; Gordon, R. G.; Palacios, T.; Gordon, R. G. *Appl. Phys. Lett.* **2012**, *101* (23), 232109.

(7) Wang, X.; Dong, L.; Zhang, J.; Liu, Y.; Ye, P. D.; Gordon, R. G. *Nano Lett.* **2013**, *13* (111), 594−599.

(8) Hellman, E. S.; Hartford, E. H. *Appl. Phys. Lett.* **1994**, *64* (11), 1341−1343.

(9) Paisley, E. A.; Gaddy, B. E.; Lebeau, J. M.; Shelton, C. T.; Biegalski, M. D.; Christen, H. M.; Losego, M. D.; Mita, S.; Collazo, R.; Sitar, Z.; Irving, D. L.; Maria, J.-P. P. *J. Appl. Phys.* **2014**, *115* (6), 064101.

(10) Chen, J.-J.; Hlad, M.; Gerger, A. P.; Gila, B. P.; Ren, F.; Abernathy, C. R.; Pearton, S. J. *J. Electron. Mater.* **2007**, *36* (4), 368−372.

(11) Gila, B. P.; Hlad, M.; Onstine, A. H.; Frazier, R.; Thaler, G. T.; Herrero, A.; Lambers, E.; Abernathy, C. R.; Pearton, S. J.; Anderson, T.; Jang, S.; Ren, F.; Moser, N.; Fitch, R. C.; Freund, M. *Appl. Phys. Lett.* **2005**, *87* (16), 163503.

(12) Wang, X. Applications of Vapor Deposition in Microelectronics and Dye-Sensitized Solar Cells, Harvard University, 2013.

(13) Kim, S. B.; Yang, C.; Powers, T.; Davis, L. M.; Lou, X.; Gordon, R. G. *Angew. Chem., Int. Ed.* **2016**, *55*, 10228−10233.

(14) de Rouffignac, P.; Sullivan, N.; Beaulieu, D.; Park, J.-S.; Hock, A.; Gordon, R. G. Proceedings of the AVS Atomic Layer Deposition Conference, 2009.

(15) Doman, R. C.; Barr, J. B.; Mcnally, R. N.; Alper, A. M. *J. Am. Ceram. Soc.* **1963**, *46*, 313−316.

(16) Li, H. D.; Zhang, X. N.; Zhang, Z.; Mei, Z. X.; Du, X. L.; Xue, Q. K. *J. Appl. Phys.* **2007**, *101* (10), 106102.

(17) Gila, B. P.; Thaler, G. T.; Onstine, A. H.; Hlad, M.; Gerger, A.; Herrero, A.; Allums, K. K.; Stodilka, D.; Jang, S.; Kang, B.; Anderson, T.; Abernathy, C. R.; Ren, F.; Pearton, S. J. *Solid-State Electron.* **2006**, *50* (6), 1016−1023.

(18) Matocha, K.; Gutmann, R. J.; Chow, T. P. *IEEE Trans. Electron Devices* **2003**, *50* (5), 1200−1204.

(19) Nicollian, E. H.; Goetzberger, A. *Bell Syst. Technol. J.* **1967**, *46* (6), 1055−1033.

(20) Brown, D. M.; Gray, P. V. *J. Electrochem. Soc.* **1968**, *115* (7), 760−766.

(21) Yang, S.; Tang, Z.; Wong, K. Y.; Lin, Y. S.; Liu, C.; Lu, Y.; Huang, S.; Chen, K. J. *IEEE Electron Device Lett.* **2013**, *34* (12), 1497−1499.

(22) Bin Lu, B.; Min Sun, M.; Palacios, T. *IEEE Electron Device Lett.* **2013**, *34* (3), 369−371.

DOI: 10.1021/acs.nanolett.6b03638
Nano Lett. 2016, 16, 7650−7654